QUANTITATIVE VALIDATION OF AN AUTOMATIC SEGMENTATION METHOD FOR IDENTIFICATION OF THE REGIONS OF INTEREST IN INTRAVASCULAR ULTRASOUND IMAGES

C.V. Bourantas, D.I. Fotiadis, L.K. Michalis, M.E. Plissiti,
V. Protopappas, G.V. Mpozios, C.K. Katsouras and I.C. Kourtis

22– 2002

Preprint, no 22 – 02 / 2002

Department of Computer Science
University of Ioannina
45110 Ioannina, Greece

Quantitative Validation of an Automatic Segmentation Method for Identification of the Regions of Interest in Intravascular Ultrasound Images

C.V. Bourantas[(1)], D.I. Fotiadis[(2)], L.K. Michalis[(1),*], M.E. Plissiti[(2)], V.Protopappas[(2)], G.V. Mpozios[(1)], C.K. Katsouras[(1)] and I.C. Kourtis[(2)]

[(1)] Dept. of Cardiology, Medical School, University of Ioannina, GR 45110 Ioannina Greece

[(2)] Dept. of Computer Science, Unit of Medical Technology and Intelligent Information Systems, University of Ioannina, GR 45110 Ioannina Greece

---

[*]Corresponding author

Department of Cardiology, Medical School, University of Ioannina, GR 451 10 Ioannina, GREECE

PO Box 1186

tel.: +30 651 98820, fax: +30 651 98889

e-mail: lmihalis@cc.uoi.gr

Running Title: Validation of an IVUS Image Segmentation Method

Quantitative Validation of an Automatic Segmentation Method for Identification of the Regions of Interest in Intravascular Ultrasound Images

Abstract

We have developed a new automatic border detection method for the fast and accurate detection of lumen, media – adventitia and stent borders in coronary arteries from Intravascular Ultrasound (IVUS) images. The method is based on the use of deformable models whose energy is minimized using a Hopfield Neural Network. The detection of the borders is accompanied by several correction techniques to overcome problems related to the quality of IVUS frames. We validate the developed method against two expert observers in a dataset of 80 IVUS frames. We estimate several metrics including the interobserver variability of our method for area and perimeter, parameters of linear regression analysis (slopes, y – interceptions, correlation coefficients) and the Williams Index (WI) for area, perimeter, non-overlapping areas, Hausdorff distance and mean distance. Our results demonstrate that the proposed method is reliable, accurate and capable to identify rapidly the regions of interest in sequences of IVUS frames.

Key Words: Intravascular Ultrasound; IVUS segmentation; validation.

1. INTRODUCTION

Intravascular ultrasound (IVUS) is a relatively new method, which generates cross – sectional images of coronary arteries with high temporal and spatial resolution. The method is used for the evaluation of vessel wall morphology and dimensions (De Feyter et al. 1991; Hodgson et al. 1190; Gerber et al. 1994; Mallery et al. 1990; Neville et al. 1989; Nishimura et al. 1990; Nissen et al. 1991; Potkin et al. 1990) Furthermore, IVUS provides data about the composition of the atheromatus plaque (Flank et al. 1995). This is useful in the prognosis of coronary artery disease, as lesions prone to rapture can be identified. During the past decade IVUS has become an important tool in both clinical and research applications.

IVUS requires the insertion, within the coronary artery, of a catheter with a transducer on its tip. The transducer transmits a high frequency (20 – 40 MHz) ultrasound signal perpendicular to the catheter axis. The catheter is attached to a motorized pullback device in order to be moved with a constant speed on a stable pullback path, which is determined by the vessel's curvature. Cross – sectional images are generated due to the attenuation of the signal while it is passing through the vessel wall. Subsequently, a sequence of IVUS images is obtained. In each image, lumen (e.g. lumen cross sectional area), external elastic membrane (e.g. external elastic membrane cross sectional area – in the text the term media – adventitia border is used), atheroma (e.g. plaque burden), calcium, stent (e.g. stent cross sectional area) and remodeling (e.g. positive remodeling) measurements can be made (Mintz et al. 2001).

However, there are several IVUS artifacts, which reduce the ability to identify vessel wall layers and influence the accuracy of the obtained measurements. Those artifacts are: (a) ring –down, blood speckle and near field artifacts, (b) transducer obliquity and vessel curvature and (c) spatial catheter orientation.

Border detection in IVUS images is done manually. This process is laborious, time consuming and can be unreliable in the hands of an inexperienced operator (Meier et al. 1997). As a result these problems have restricted its clinical application. To overcome these drawbacks and enhance IVUS utilization, we developed a novel

method, which identifies accurately and quickly the different layers of the vessel wall (Plissit et al. 2001). The aim of the present study is to validate this novel method.

2. MATERIALS AND METHODS

Intravascular Ulrasound

The IVUS images were obtained using a 30-MHz catheter (Avanar F/X, Endosonics, USA, catheter size 2.9 F, length 150 cm). Sequential imaging was obtained with the IVUS catheter been connected to a motorized pullback device operating at a speed of 0.5 mm/sec. IVUS images were acquired at a standard rate of 10 frames/sec and were digitized in DICOM format. The calibration markers, displayed on the digitized images, were used to derive the pixel size of 0.017mm, which was used to calculate the cross – sectional areas and the perimeters of the different regions of interest.

Study Group

We analyzed sequences of images from coronary artery segments of 10 patients, who underwent IVUS examination for clinical purposes. The analyzed segments located in the left anterior descending artery (3), right coronary artery (5) and left circumflex coronary artery (2). In 5 out of 10 assessed coronary arteries stent implantation preceded the IVUS examination. From each IVUS examination 60sec were digitized.

From the digitized IVUS examination 80 randomly selected IVUS frames, spaced > 1.5mm between each other, were finally used for the validation of our method. As a condition for inclusion, frames had to belong in angiographically relatively straight coronary artery segments without side branches and no calcification encompassing $>30^{o}$ of the arterial circumference.

Automated IVUS Border Detection Method

The acquired IVUS images are preprocessed to remove noise. A 3×3 median filter was applied to eliminate the effect of artifacts and speckles. A linear filter was used for image enhancement.

The automated segmentation method was based on the principles of deformable models (snakes). Initially an expert observer provided an estimation regarding the regions of interest of the first IVUS image of each sequence of images. The lumen and media – adventitia borders in the following frames of the sequence were automatically extracted using information from the previous image.

The position of the snake is represented parametrically by $v(s) = (x(s), y(s))$, and its energy functional can be written as:

$$E_{\text{snake}} = \int_0^1 \left(E_{\text{int}}(v(s)) + E_{\text{image}}(v(s))\right) ds \,, \tag{1}$$

where E_{int} represents the internal energy of the snake due to bending and E_{image} is derived from the image data (Kass et al. 1987). As in most conventional snake models, the internal energy is a function of the first and second order derivatives of the curve, and can be expressed as:

$$E_{\text{int}} = \alpha(s)\left|v'(s)\right|^2 + \beta(s)\left|v''(s)\right|^2 . \tag{2}$$

E_{image} forces the snake to be attracted to image features, and it is defined as:

$$E_{\text{image}} = -\gamma(s)\left|\nabla I\right|^2 , \tag{3}$$

where $|\nabla I|$ is the image gradient.

In the discrete domain the energy functional of the snake takes the form:

$$E_{\text{snake}} = \sum \left\{ \alpha \left[(x_i - x_{i-1})^2 + (y_i - y_{i-1})^2 \right] + \beta \begin{bmatrix} (x_{i-1} - 2x_i + x_{i+1})^2 \\ + (y_{i-1} - 2y_i + y_{i+1})^2 \end{bmatrix} - \gamma g_i \right\}, \qquad (4)$$

where N is the number of points of the snake and g_i is the image gradient at the point i of the image.

In order to construct a searching space where the snake can deform, the center of the curve drawn by the expert observer is determined and N points from the curve are selected at equal angles of 15°. Then perpendicular to the curve line segments consisted of M points are drawn at each sample point. The points that construct those line segments are the candidate points of the final contour. At each line segment, the point that minimizes the energy function of the snake is selected.

The energy of the snake is minimized using a Hopfield neural network. A typical Hopfield network consists of a single layer of neurons. Each node has a bias I and is connected with every other node. The connections are bi-directional and symmetric and a specific weight T_{ij} is assigned to each connection. The state u_i of the i neuron depends on the input it receives from other neurons and is expressed as:

$$u_i = \sum_{j=1}^{N} T_{ij} o_j + I_i, \qquad (5)$$

where N is the number of neurons and o_i each neuron's output, which takes the values 0 or 1 (firing or not firing). The Hopfield network converges when the energy functional reaches a local minimum. The total energy functional is given as:

$$E = -\frac{1}{2}\sum_{i=1}^{N}\sum_{j=1}^{N} T_{ij} o_i o_j - \sum_{i=1}^{N} I_i o_i \,. \tag{6}$$

In our case the network consists of one layer of $N \times M$ neurons. Each neuron $(i, j)\,(1 \le i \le N, 1 \le j \le M)$ represents a candidate point of the final curve.

The energy of the snake that will be finally minimized is:

$$E = \sum_{i=1}^{N} \left\{ \begin{array}{l} \alpha\left[\left(\sum_{k=1}^{M} x_{ik} o_{ik} - \sum_{k=1}^{M} x_{i-1k} o_{i-1k} \right)^2 + \left(\sum_{k=1}^{M} y_{ik} o_{ik} - \sum_{k=1}^{M} y_{i-1k} o_{i-1k} \right)^2 \right] + \\ \beta\left[\begin{array}{l} \left(\sum_{k=1}^{M} x_{i-1k} o_{i-1k} - 2\sum_{k=1}^{M} x_{ik} o_{ik} + \sum_{k=1}^{M} x_{i+1k} o_{i+1k} \right)^2 + \\ \left(\sum_{k=1}^{M} y_{i-1k} o_{i-1k} - 2\sum_{k=1}^{M} y_{ik} o_{ik} + \sum_{k=1}^{M} y_{i+1k} o_{i+1k} \right)^2 \end{array} \right] - \\ \gamma\left[\sum_{k=1}^{M} g_{ik} o_{ik} \right] \end{array} \right\} \tag{7}$$

where x, y are the coordinates of a point, o is the output of a neuron and g is the image energy. The interconnective strengths are given as:

$$T_{ikji} = \left| (4\alpha + 12\beta)\delta_{ij} - (2\alpha + 8\beta)\delta_{i+1\,j} - (2\alpha + 8\beta)\delta_{i-1\,j} + 2\beta\delta_{i+2\,j} + 2\beta\delta_{i-2\,j} \right| \left[x_{ik} x_{ji} + y_{ik} y_{ji} \right], \tag{8}$$

where:

$$I_{ik} = \gamma g_{ik} \text{ and } \delta_{ij} = \begin{cases} 1, \text{if } i = j \\ 0, \text{otherwise} \end{cases}.$$

Since the weight and the bias of each connection are computed, the above relations determine the state and output of each neuron. The state of a neuron, which is considered as a firing neuron, is acceptable only if the total energy of the network is diminished. The neurons, which are considered as firing neurons, define the borders of the regions of interest.

In many cases the proposed method is difficult to detect the regions of interest due to the quality of the IVUS images. To improve the efficiency of the method, we consider more appropriate to detect smooth edges that separate large regions, which contain pixels of similar intensity. Thus, the gradient for each pixel of the image is defined as:

$$g_i = \sqrt{(\bar{u}_i - \bar{b}_i)^2 + (\bar{l}_i - \bar{r}_i)^2}\,, \tag{9}$$

where $\bar{u}_i, \bar{b}_i, \bar{l}_i$ and $\bar{r}_i$ are the mean values of the intensity of the pixels in the upper, bottom, left and right neighborhood of the pixel i, respectively. With this modification the network converges at points that minimize the total energy of the snake and define the boundary of the region of interest.

In addition, for the correct detection of media – adventitia border a smooth initial estimation is needed. We calculated the convex hull of the final points of the snake. In this way, we avoided abnormalities in the specification of the searching area, which are caused by small distortion in the shape of the detected contour in the previous frame.

The above method was applied twice for each sequence of IVUS frames in order the lumen initially and the media - adventitia border afterwards to be detected.

Method of Validation

Ideally, in order an IVUS boundary detection method to be reliable the borders that the method detects should be the same with the "real" borders. However, the "real" location of these borders is not known. Previous studies have shown that histology cannot provide accurate information regarding the borders' location, due to the

shrinkage of the tissues and the inability to determine the precise correspondence between IVUS images and histological slices (Mallery et al. 1990). Therefore, only by comparing the region of interest that a method identifies with those been detected by expert observers the accuracy of a border detection method can be ascertained. For this purpose, usually two expert observers trace twice the IVUS images and the average of area and perimeter values is utilized as the golden standard.

In our case, 2 expert observers examined the 80 randomly selected frames used for the validation of our method and the lumen, media – adventitia borders were traced. Forty of the examined frames were obtained from stented coronary artery segments and as a result the experts, although they were traced the stent, were unable to detect the media – adventitia border in 22 of them. The IVUS frames were examined twice and with a month's interval between each one of the examinations.

The regions of interest (lumen, media – adventitia border, stent) computed by our automated method were compared with those been traced by the experts.

The reliability and reproducibility of manual tracing was assessed by estimating the inter – and intra – observer variability for area and perimeter of the regions of interest. Inter - and intra – observer variability were defined as (Kovalski et al. 2000):

Inter variability:

$$V_1 = 100 \sum^{N} \frac{|A_1 - A_2|}{\frac{A_1 + A_2}{2}}, \qquad (10)$$

where A_1 and A_2 represent the values of area/perimeter obtained from the first and second tracing, respectively, and N is the number of IVUS images.

Intra variability:

$$V_{intra} = 100 \sum^{N} \frac{|A - B|}{\frac{A + B}{2}}, \qquad (11)$$

where $A = \frac{A_1 + A_2}{2}$ and $B = \frac{B_1 + B_2}{2}$.

Several ways were used to evaluate the performance of the proposed method:

a) The automated method was considered as an independent observer and the interobserver variability between manual tracing (average) and automated border detection was computed. This interobserver variability was defined as:

$$V_{alg} = 100 \sum^{N} \frac{|C_{alg} - (\frac{A+B}{2})|}{\frac{A+B}{2}}, \quad (12)$$

where C_{alg} is the area/perimeter computed by the proposed method.

b) Linear regression analysis was also used (Bland et al. 1986). Correlation coefficients, slope and y – interception were computed to compare the areas and perimeters estimated by the automated boundary detection method and the average of the two experts.

c) The proposed automated boundary detection method was judged in the context of interobserver variability and the Williams Index (WI) (Chalana et al. 1997) was computed for perimeter and area. The WI was defined as:

$$\mathrm{WI} = \frac{\frac{1}{\mathrm{n}} \sum_{j=1}^{n} \frac{1}{D_{0,j}}}{\frac{2}{n-1} \sum_{j} \sum_{j' \neq j} \frac{1}{D_{j,j'}}}, \quad (13)$$

where n is the number of observers, $D_{j,j'}$ is the average disagreement between observers and $D_{0,j'}$ is the disagreement between our method and each observer. The average disagreement between the two observers is defined as:

$$D_{j,j'} = \frac{1}{N} \sum_{i=1}^{N} e(\boldsymbol{x}_{ij}, \boldsymbol{x}_{ij'}), \quad (14)$$

where $\boldsymbol{x}_{ij}$ is a vector observation on subject i by an observer j, N is the number of subjects, and the function $e(\boldsymbol{x}, \boldsymbol{y})$ is a distance metric between observations, $\boldsymbol{x}$ and $\boldsymbol{y}$. The distance metric in our case is defined as the difference between the measurements of area or perimeter of the two observers.

d) Further, to make a direct comparison of area and perimeter measurements we performed nonoverlapping area analysis (Bland et al. 1986). This type of analysis leads to the redetermination of inter -, intra – and manual vs. automatic variability. In addition, we have computed the Williams Index for nonoverlapping areas.

e) Hausdorff and mean distance were utilized to determine a difference metric between the manual and the automated computed contours. The Hausdorff distance was defined as:

$$D_{Haussd} = \max_i d_i \tag{15}$$

and the mean distance as:

$$D_{\text{mean}} = \frac{1}{n}\sum_n d_i \,, \tag{16}$$

where $d_i = \sqrt{(x_i - x'_i)^2 + (y_i - y'_i)^2}$ denotes the distance between corresponding points and n denotes the number of corresponding points.

Artificial correspondence between points in the manual traced and computer obtained contour was established using an object – based method, originally used for inter-slice interpolation between consecutive tomographic images (Coshtasby et al. 1992; Protopappas 1999). In this method, each point (x,y) of the first contour (defined as reference contour) corresponds to a point (x',y') in the second contour (defined as target contour), which best matches it, using minimization of a vector cost function. This function takes into account the gradient magnitude and direction as well as the distance between the points. The function was defined as:

$$C(x,y,x',y') = u_1[D(x,y) - D'(x',y')]i + u_2[\theta(x,y) - \theta'(x',y')]j + u_3\sqrt{(x-x')^2 + (y-y')^2}k \tag{17}$$

where $D(x,y)$ and $\theta(x,y)$ are the gradient magnitude and direction, respectively, and u_1, u_2, u_3 are weights that specify the relative importance of the above three function components. Searching in a small neighborhood, in the target curve, we obtained the best matching point. Swapping the reference and the target curves and applying the above-mentioned procedure, we discarded all the incorrect matches and established

the final corresponding points. The average curve was then determined by plotting a contour at the mid-distance of the displacement between the corresponding points.

3. RESULTS

The inter - and intra – observer variability of the two experts for the lumen, media – adventititia border and stent based on the values of area and perimeter are shown in Tables 1 and 2, respectively.

The interobserver variability for our method for area and perimeter is given in Table 3. Applying linear regression analysis to the automatically obtained contours of the lumen, media – adventitia border and stent vs. the manual reference yielded slopes, y-intercept and correlation coefficient shown in Table 4. In addition, the linear regression analysis for the media – adventitia area is depicted graphically in Fig. 1. The Williams Index for area and perimeter is shown in Table 5. To compute the 95% WI confidence interval the jack – knife technique was applied (Bland et al. 1986).

The results obtained for the nonoverlapping area analysis are outlined in Table 6. The Williams Index for nonoverlapping areas is given in Table 7. The Williams Index for Hausdorff and mean distances are shown in Table 8.

4. DISCUSSION

In this paper, the validation of a novel automatic method for the lumen, media – adventitia and stent border detection from IVUS images was presented. The detection method is based on the principles of deformable models. The user interacts with the first frame in a sequence of IVUS frames to provide with an initial estimation of the border and the method can automatically extract the borders in all following frames. To minimize the deformable model energy a Hopfield Neural Network is utilized. The automatic contour detection method fails to identify the correct media – adventitia border in the IVUS frames where large side branches or calcified plaques are depicted. However, the deformable model is reinstated without manual

intervention in the IVUS frames, which follow, where these disorientating factors are not pictured. The proposed method proves to be very efficient and fast compared with manual intervention, which is slow, tedious and non-reproducible.

The clinical application of the method can be questioned as there is no previous knowledge of its accuracy and reliability. For this purpose we performed validation of the proposed method. Two experts traced twice 80 IVUS images and the obtained contours were compared with the ones obtained by the application of our method. Several metrics have been such as the automated method interobserver variability, the Williams Index for area and perimeter, Hausdorff and mean distance of curves. This has been achieved applying direct comparison, linear regression analysis and nonoverlapping area analysis. The analysis indicates that the accuracy and reliability of our method is high.

The reliability of the two observers is assessed using inter - and intra – observer variability. Intra – observer variability for area ranges from 1.59 % - 2.84 %, for perimeter from 1.04 % - 2.22 % and for non-overlapping areas from 1.57 % - 2.72 %. The above values compare well with others reported in the literature (Kovalski et al. 2000; Meier et al. 1997).

Linear regression analysis results indicate that the method is accurate. The slopes are close to unity, the y – interception confidence interval includes always zero and the correlation coefficient is higher than 0.98 in all cases. The worst performance according to linear regression is obtained for the perimeter of the stent. The proposed method will deviate more in regions (e.g. stent), which are easily detected by the observers. However, the performance of the method is good enough.

The automated method was considered in our validation approach as an independent observer and the Williams Index can provide with a qualitative measure of the accuracy of the method. Williams Index values close to unity indicate that the method is accurate. WI for area ranges from 0.67 – 0.91 and for perimeter from 0.73 – 0.84. WI for area is low for the media – adventitia border and high for lumen. For the perimeter the lowest value is obtained for stent and the highest for lumen. This is

due to the fact that observers can easier detect the media – adventitia border and stent. WI for non-overlapping areas ranges from 0.79 – 0.91. The lower value is obtained for media – adventitia border followed by the stent. WI for Hausdorff distance ranges from 0.88 – 0.90 and the WI for mean distance from 0.82 – 0.90. The later indicates that statistically our method is accurate. In general, the lumen detection using the proposed method is more accurate than the detection of media – adventitia and stent.

The obtained WI for the lumen is higher than the WI obtained for the stent. This is contrast with the interobserver variability, which for the proposed method is higher for the lumen. This can be due to the low intra – observer variability (2.01%$\pm$1.56) which affects more the Williams Index.

Inter – observer variability has not been taken into account in previous studies. In our case its value is low, which implies that the WI value is low. The obtained for our method high values of WI index under these circumstances indicate that the proposed method is highly reliable. This must be taken into account in the media – adventitia border detection (case of low WI).

The task of identifying the regions of interest in IVUS images is a challenging issue. Several algorithms have also been developed to trace the lumen and media-adventitia borders (Hagenaars et al. 2000; Klingensmith et al. 2000; Kovalski et al. 2000; Mojsilovic et al. 1997; Shekhar et al. 1999) and several attempts to examine their reliability have been presented. The validation results for our underline its high performance designate the proposed method as one of the most efficient and accurate method for IVUS segmentation. We have not validated our method in terms of computer time needed for border detection, but it seems that it is fast need, since no more that 45 min is requested for a sequence of 600 IVUS frames on Pentium 4, 1.2 GHz.

However, the proposed method has several limitations, which must be addressed in the future. One of these is that the algorithm fails to identify the lumen and media – adventitia border in the IVUS frames in the presence of side branches or echogenic calcified plaque. Our automated method includes also three – dimensional reconstruction of the coronary arteries and its validation will be presented in a future

communication. Three-dimensional reconstruction makes it feasible to assess fast and accurately in the same arterial segment, changes in the lumen and plaque volume and to estimate the influence of intervening treatment or pharmacological agents in the regression of atherosclerosis.

5. CONCLUSIONS

IVUS provides tomographic views with precise morphology and geometry of arterial segments, which is not possible with contrast angiography or any other image modality. For fast and accurate extraction of the regions of interest in IVUS frames, an automatic method was developed. In this paper we have described a validation methodology, which thoroughly estimates the accuracy and the reliability of the proposed method. The results confirm its efficiency in determining lumen and media-adventitia border and nominate our method as one of the most robust methods for IVUS segmentation.

Thus, the automated method may have clinical use. Up to date the IVUS segmentation has been restricted as it involves manually tracing which is tedious non-reproducible and time consuming. The proposed method overcomes the aforementioned difficulties and extends the clinical applicability of IVUS imaging.

References

Bland JM, Altman DG. Statistical methods for assessing Agreement between two methods of clinical measurement. The Lancet 1986; 1(8476): 307 – 310.

Chalana V and Kim Y. A methology for evaluation of boundary detection algorithm on medical images. IEEE Trans Med Imaging 1997; 16(5): 642 – 652.

De Feyter PJ, Serruys PW, Davies MJ, Richardson P, Lubsen J, and Oliver MF. Quantitative coronary angiography to measure progression and regression of coronary atherosclerosis. Value, limitations, and implications for clinical trials. Circulation 1991; 84: 412-423.

Flank E, Shah PK, and Fuster V. Coronary plaque disruption. Circulation 1995 ; 92 : 657 –671.

Gerber TC, Elber R, Gorge G, Ge J, Rupprecht HJ, Meyer J. Extent of atherosclerosis and remodeling of the left main coronary artery determined by intravascular ultrasound. Am. J. Cardiol 1994; 73(9): 666 – 671.

Goshtasby A, Turner DA and Ackerman LV. Matching of Tomographic Slices for Interpolation. IEEE Trans Med Imaging 1992; 11(4): 507-516.

Hagenaars T, Gussenhoven EJ, Van Essen JA, Seelen J, Honkoop J, and Van der Lugt A. Reproducibility of volumetric quantification in intravascular ultrasound images. Ultrasound Med Biol 2000; 26(3): 367 – 374.

Hodgson JM, Graham SP, Sheehan H, Savakus AD. Percutaneus intracoronary ultrasound imaging: initial applications in patients. Echocardiography 1990; 7(4): 403 - 413.

Kass M, Witkin A, Terzopoulos D. Snakes: "Active contour models". International Journal of Computer Vision 1987; 1: 321 – 331.

Klingensmith JD, Sheknar R, and Vince DG. Evaluation of three – dimensional segmentation algorithms for the identification of luminal and medial – adventitial borders in Intravascular Ultrasound images. IEEE Trans on Medical Imaging 2000; 19(10): 996-1011.

Kovalski G, Beyear R, Shofti R and Azhari H. Three – dimensional automatic quantitative analysis of intravascular ultrasound images. Ultrasound Med Biol 2000; 26(4): 527 – 537.

Mallery JA, Tobis JM, Griffith J, Gessert J, McRay M, Moussabeck O, Bessen M, Moriouchi M, and Henry WL. Assessment of normal and atherosclerotic arterial wall thickness with an intravascular ultrasound imaging catheter. Amer Heart J 1990; 119: 1392 – 1400.

Meier DS, Cothren RM, Vince DG, and Cornhill JF. Automated morphometry of coronary arteries with digital image analysis of intravascular ultrasound. Amer Heart J 1997; 133: 681 – 690.

Mintz GS, Nissen SE, Anderson WD, Bailey SR, Elber R, Fitzgerald PJ, Pinto FJ, Rosenfield K, Siegel RJ, Tuzcu EM, Yock PG. American college of cardiology clinical expert consensus document on standards for acquisition, measurement and reporting of intravascular ultrasound studies: a report of the American College of Cardiology task force on clinical expert consensus documents (committee to develop a clinical expert consensus on standards for acquisition, measurement and reporting of intravascular ultrasound studies [IVUS]). J of Am Coll of Cardiology 2001; 37: 1478 – 1492.

Mojsilovic A, Popovic M, Amodaj N, Babic R, Ostojic M. Automatic segmentation of intravascular ultrasound images: A texture – based approach. Ann Biomed Eng 1997; 25: 1059 –1071.

Neville RF, Bartorell AL, Sidawy AN, Almagor Y, Potkin B, Leon MB. An in vivo feasibility study of intravascular ultrasound imaging. Am J Surg 1989; 14(4): 947 – 952.

Nishimura RA, Edwards WD, Warnes CA, Reeder GS, Holmes DR, Tajik AJ, York PG. Intravascular ultrasound imaging: in vitro validation and pathologic correlation. J Am Coll Cardiol 1990; 16(1):145-154.

Nissen SE, Gurley JC, Grines CL, Booth DC, McClure R, Berk M, Fischer C, DeMaria AN. Intravascular Ultrasound assessment of lumen size and wall morphology in normal subjects and patients with coronary artery disease. Circulation 1991; 84: 1087–1099.

Plissiti ME, Fotiadis DI, Michalis LK. 3D Reconstruction of Stenotic Coronary Arterial Segments using Intravascular Ultrasound and Angiographic Images. XVIIIth Congress of the International Society of Biomechanics, ETH Zurich, Switzerland, July 8-13, 2001.

Protopappas V. Development and Evaluation of Interpolation Techniques for the Three-Dimensional Imaging of Human Organs. Diploma Thesis, Dept. of Electrical and Computer Engineering, National Technical University of Athens, 1999.

Potkin BN, Bartorelli AL, Gessert JM, Neville RF, Almagor Y, Roberts WC, and Leon MB. Coronary artery imaging with intravascular high-frequency ultrasound. Circulation 1990; 81: 1575-1585.

Shekhar R, Cothern RM, Vince DG, Chandra S, Thomas JD, Cornhill JF. Three – dimensional segmentation of luminal and adventitial borders in serial intravascular ultrasound images. Computerized Medical Imaging and Graphics 1999; 23: 299 – 309.

Table 1: Lumen, media adventitia border and stent area variability. Results are presented as mean ± standard deviation

Variability	Media – Adventitia N= 58	Lumen N=80	Stent N=40
Inter observer (1) variability (%)	2.06±1.67	3.61±3.64	2.88±2.06
Inter observer (2) variability (%)	1.50±1.10	2.84±2.64	2.86±2.37
Intra observer variability (%)	1.59±1.58	2.84±2.81	2.08±1.63

Table 2: Lumen, media adventitia border and stent perimeter variability. Results are presented as mean ± standard deviation

Variability	Media – Adventitia N= 58	Lumen N=80	Stent N=40
Inter observer (1) variability (%)	1.23±1.17	2.16±1.90	1.86±2.36
Inter observer (2) variability (%)	1.15±1.56	1.96±1.33	1.84±2.19
Intra observer variability (%)	1.04±1.10	1.69±1.67	1.16±1.59

Table 3: Interobserver variability of the proposed method. Results are presented as mean ± standard deviation

	Media – Adventitia N= 58	Lumen N=80	Stent N=40
Area	2.22±1.60	2.80±2.92	2.34±1.70
Perimeter	1.21±0.81	1.88±1.53	1.47±1.16

Table 4: Slope, 95% confidence interval of slope, y – interception, 95% confidence interval of y – intercept and correlation coefficient for areas and perimeters.

	Slope	CI (95%)	y intercept	CI (95%)	Correlation coefficient
Media – Adventitia (area)	1.03	(1.00,1.06)	-0.08 mm^2	(-0.77,0.61) mm^2	0.99
Media – Adventitia (perimeter)	1.03	(1.00,1.06)	-0.26 mm	(-0.29,-0.23) mm	0.99
Lumen (area)	0.97	(0.92, 1.02)	0.14 mm^2	(-0.09,0.37) mm^2	0.99
Lumen (perimeter)	0.97	(0.91, 1.03)	0.14 mm	(-0.22,0.50) mm	0.99
Stent (area)	0.99	(0.94,1.04)	0.07 mm^2	(-0.09,0.23) mm^2	0.99
Stent (perimeter)	0.94	(0.83,1.05)	0.28 mm	(-0.37,0.93) mm	0.98

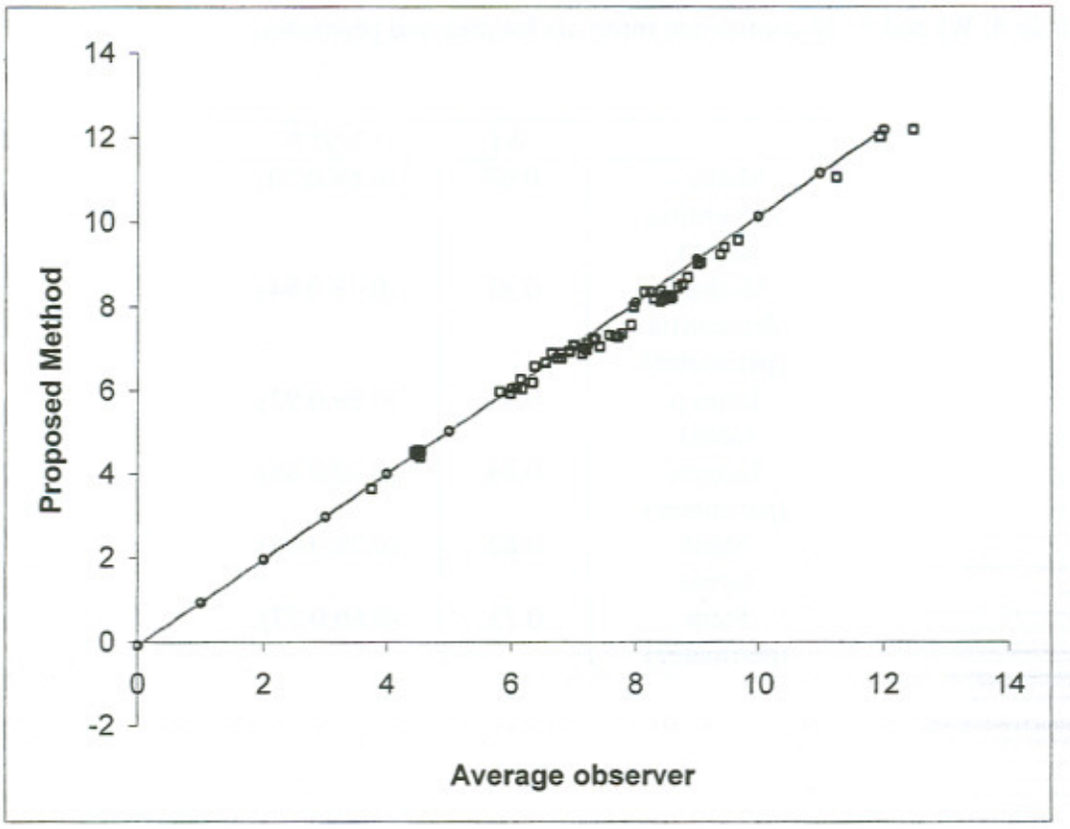

Figure 1: Linear regression analysis of the automatic media – adventitia area vs. manual tracing.

Table 5: WI and 95 % confidence intervals for area and perimeter.

	WI	CI(95%)
Media – Adventitia (area)	0.67	(0.64,0.70)
Media – Adventitia (perimeter)	0.81	(0.78,0.84)
Lumen (area)	0.91	(0.89,0.93)
Lumen (perimeter)	0.84	(0.82,0.86)
Stent (area)	0.82	(0.78,0.86)
Stent (perimeter)	0.73	(0.69,0.77)

Table 6: Inter - and intra – observer variability for non-overlapping areas. Results are presented as mean ± standard deviation

Variability	Media – Adventitia N= 58	Lumen N=80	Stent N=40
Inter observer (1) variability (%)	3.88±1.38	6.64±3.88	5.16±2.16
Inter observer (2) variability (%)	3.62±0.92	5.95±2.47	5.58±2.12
Intra observer variability (%)	1.57±1.59	2.72±2.80	2.01±1.56
Interobserver (Automated method) variability	4.11±2.81	6.03±4.45	4.99±1.39

Table 7: WI and 95% confidence intervals for the non-overlapping areas.

	WI	CI (95%)
Media – Adventitia	0.79	(0.77,0.81)
Lumen	0.91	(0.90,0.92)
Stent	0.82	(0.81,0.83)

Table 8: WI and 95% confidence interval for Hausdorff distance and mean distance.

	WI	CI (95%)
Media – Adventia (Hausdorff distance)	0.88	(0.87,0.89)
Lumen (Hausdorff distance)	0.88	(0.87,0.89)
Stent (Hausdorff distance)	0.90	(0.88,0.92)
Media – Adventia (mean distance)	0.89	(0.88,0.90)
Lumen (mean distance)	0.90	(0.89,0.91)
Stent (mean distance)	0.82	(0.81,0.83)